Title: Enhanced Astrocyte Responses are Driven by a Genetic Risk Allele Associated with Multiple Sclerosis

Authors: Gerald Ponath[1], Matthew R. Lincoln[1,2,3], Somiah Dahlawi[1], Mayyan Mubarak[1], Tomokazu Sumida[1,2,3], Laura Airas[4], Shun Zhang[5], Cigdem Isitan[1], Thanh D. Nguyen[5], Cedric S. Raine[6], David A. Hafler[1,2,3] and David Pitt[1]*

Affiliations:

[1]Department of Neurology, Yale School of Medicine, New Haven, CT 06511, USA

[2]Department of Immunobiology, Yale School of Medicine, New Haven, CT 06511, USA

[3]Broad Institute of MIT and Harvard University, Cambridge, MA 02141, USA

[4]Division of Clinical Neurosciences, University of Turku, Turku, Finland

[5]Department of Radiology, Weill Cornell Medical College, New York, NY 10021, USA

[6]Department of Pathology, Albert Einstein College of Medicine, Bronx, NY 10461, USA

*Correspondence to: David Pitt, M.D. Department of Neurology, Yale School of Medicine, New Haven, CT 06511, USA. Email: david.pitt@yale.edu

One Sentence Summary:

The NF-κB relevant multiple sclerosis risk variant, rs7665090-G, drives astrocyte responses that promote lesion formation.

Abstract: Epigenetic annotation studies of genetic variants associated with multiple sclerosis (MS) risk suggest that dysfunctional lymphocyte responses drive MS susceptibility. It remains unclear whether MS risk variants impact cellular function in the central nervous system (CNS) and whether this plays a role in MS susceptibility. Here, we investigated the effect of the risk variant, rs7665090-G, located near the *NFKB1* gene, on astrocyte function. In human fetal astrocytes, we found that chromatin was accessible at the rs7665090 locus, suggesting a potential impact of the risk variant on astroglial function. In astrocytes differentiated from MS patient-derived induced pluripotent stem cells (iPSCs), and in astrocytes within autopsied MS lesions, the risk variant was associated with increased NF-κB signaling and expression of NF-κB target genes that promote lymphocyte recruitment and neurotoxicity. Consistent with these findings, infiltrating lymphocytes were increased in MS lesions homozygous for the risk variant. Moreover, in MS patients, the rs7665090 risk variant was associated with increased total lesion volumes on magnetic resonance imaging (MRI).

Overall, our work establishes that the rs7665090-G variant directly perturbs CNS cell function, resulting in enhanced lymphocyte recruitment and reduced thresholds for lesion formation. Thus, MS may be triggered by a complex interplay between the peripheral immune system and the CNS, where dysfunctional peripheral immune responses are targeted to the CNS e.g. through enhanced astrocytic responses.

Introduction: Multiple sclerosis (MS) is a genetically mediated inflammatory disease of the central nervous system (CNS), where infiltrating immune cells lead to focal, demyelinating lesions *(1)*. Genome-wide association studies (GWAS) have now identified over 200 genetic variants associated with increased risk of developing MS *(2)*. A recent epigenetic annotation study has demonstrated that MS risk variants are highly enriched in immune enhancers, active in T and B cells *(3)*, suggesting that risk variant-mediated MS susceptibility is driven by changes in gene regulation in lymphocytes. This was confirmed in our recent work where we prioritized up to 551 potentially associated MS susceptibility genes and found that they implicate multiple innate and adaptive pathways distributed across different cells of the immune system *(2)*. It remains unclear whether genetic variants impact only immune processes or also affect CNS cell function, thereby conferring MS risk through CNS-intrinsic pathways.

We addressed this question by investigating how a common MS risk variant, rs7665090-G, whose relevance for NF-κB signaling has been recently established in lymphocytes *(4)*, may affect astrocytes. NF-κB is a master regulator of the innate and adaptive immunity but also controls functions such as cell survival, differentiation, and proliferation *(5)*. NF-κB plays a critical role in autoimmunity, including MS, where 18% of allelic MS risk variants are estimated to affect the NF-κB signaling pathway *(4, 6)*. Astrocytes are the main cell type that controls entry of peripheral immune cells into the CNS *(7)*, by forming a functional barrier to the CNS, thereby limiting entry of peripheral immune cells into the CNS, and by mounting pro-inflammatory responses that lead to leukocytes recruitment. In MS, astrocytes are pivotal for the formation of MS lesions *(8-10)*, and astrocyte-specific inhibition of NF-κB has been shown to dramatically ameliorate immune infiltration and tissue damage in experimental autoimmune encephalomyelitis (EAE), an animal model of MS *(11, 12)*, suggesting that variants relevant to NF-κB may alter astrocyte responses and astrocyte-mediated MS lesion pathology.

The rs7665090 risk variant tags a haplotype block of more than 90 variants that are in tight linkage disequilibrium. The haplotype block spans a large number of gene regulatory elements and

lies within *MANBA* and the intergenic space between *NFKB1* and *MANBA* as mapped by the ENCODE project (fig. 1) *(4, 13, 14)*. The rs7665090-G variant increases the odds ratio for MS susceptibility by 1.09 per G allele carried *(6)*.

Results: We assessed chromatin accessibility within the *NFκB1-MANBA* risk haploblock in astrocytes, we performed an assay for transposase-accessible chromatin with high throughput sequencing (ATAC-seq) on FACS-sorted unstimulated and stimulated human fetal and iPSC-derived astrocytes and for comparison, on *ex vivo*, unstimulated human effector and regulatory T cells *(15)*. Open chromatin sites captured by ATAC-seq were highly congruent throughout the haploblock in both astrocytes and T cells (fig.1), suggesting that the risk haploblock-associated increase in NF-κB signaling, shown previously in T cells *(4)*, may also apply to astrocytes. The specificity of our data set was confirmed by demonstrating highly divergent chromatin accessibility between astrocytes and T cells in lineage-specific genes (GFAP, CD2) and in a control haplotype block located within *NFKB1*, that confers risk for inflammatory bowel disease and systemic scleroderma but not MS (fig. S1).

Next, we determined the impact of the rs7665090 risk variant on NF-κB signaling in iPSC-derived astrocytes generated from fibroblasts of MS patients that are homozygous either for the risk (rs7665090-GG) or protective variant (rs7665090-AA) (fig. S7). In unstimulated astrocytes, NF-κB signaling was low in both groups, as measured by degradation of inhibitor of NF-κBα (IκBα) and phosphorylation of p65. Treatment of astrocytes with a combination of TNFα and IL-1β, cytokines that induce or enhance NF-κB signaling and play a major role during MS lesion development *(16-18),* increased NF-κB activation in both groups; however, NF-κB activation was significantly higher in astrocytes carrying the risk variant (fig. 2, A and B). In addition, at a resting state, expression of NF-κB p50 but not of p65 was higher in astrocytes with the risk variant compared to astrocytes with the protective variant. After stimulation, both p50 and p65 expression was substantially upregulated, again significantly higher in astrocytes with the risk variant (fig. 2C).

We then examined the effects of the risk variant on expression of a panel of 84 NF-κB target genes. Stimulation resulted in significant upregulation of 23 genes in astrocytes with the protective variant and 28 genes in astrocytes with the risk variant compared to baseline. Transcripts that were differentially expressed by 2-fold or higher ($p \leq 0.05$) in astrocytes with the risk compared to the protective variant were IL-15, ICAM1, CXCL10, CCL5 and complement component 3 (C3) (fig. 2, D, E and S2). Upregulation of protein expression was confirmed with ELISA or Western blot (fig. 2F and S2). These findings indicate that the rs7665090 risk variant activates a specific set of NF-κB target genes in reactive astrocytes that facilitates lymphocyte recruitment and activation. Moreover, risk variant-induced upregulation of C3 suggests astrocytic polarization towards a recently described toxic phenotype, termed A1 in analogy to M1 macrophages, for which C3 is the main marker *(19)*.

We subsequently investigated whether the risk variant impacts on homeostatic and metabolic functions of astrocytes, namely glutamate transport and uptake/release of glucose and lactate. Glutamate uptake was robust in unstimulated iPSC-derived astrocytes in both groups and deteriorated with proinflammatory stimulation, as described previously *(20)*. Removal of glutamate was marginally but significantly more impaired in iPSC-derived astrocytes with the risk compared to astrocytes with the protective variant (fig. 2G). Glucose uptake did not differ between stimulated and unstimulated astrocytes with either variant, while release of lactate was slightly but significantly diminished in astrocytes with the risk variant after stimulation but not at baseline (fig. 2, H and I).

Having determined the effect of the rs7665090 risk variant on astrocytes *in vitro*, we asked whether comparable phenotypic changes can be seen in reactive astrocytes in MS lesions. From a total of 14 MS autopsy cases homozygous for either the risk or the protective variant (fig. S7), we identified 10 cases with chronic active white matter lesions, i.e. lesions with demyelinated lesion centers and lesion edges that contained activated microglia, macrophages and hypertrophic astrocytes (fig. 3A). For comparison of astrocytic phenotypes associated with the rs7665090 risk

and protective variant, we selected lesions with similar $CD68^+$ cell densities at the lesion rim (fig. 3, A and B). Confocal imaging of immunofluorescent-labeled sections demonstrated significant and substantial upregulation of NF-κB p50 and p65 in the cytosol and nuclei of hypertrophic $GFAP^+$ astrocytes in lesions with the risk variant, the latter being indicative of NF-κB activation (fig. 3, C and D). Antibodies against phosphorylated p65 were not applied, since protein phosphorylation decays rapidly in *post mortem* tissue, making p65 phosphorylation an unreliable marker for NF-κB signaling *(21)*. Both proteins were near absent in non-reactive astrocytes in the lesion vicinity and in normal appearing white matter, suggesting low levels of NF-κB expression in non-activated astrocytes.

Furthermore, immunofluorescent staining for CXCL10, CCL5, IL-15, ICAM1 and C3d showed substantial upregulation in hypertrophic astrocytes in lesions with the risk variant (fig. 3, E-G, and S3), as predicted by our results in iPSC-derived astrocytes. As in iPSC-derived astrocytes, a specific set of NF-κB target genes was upregulated, while other markers of astroglial activation (GFAP, iNOS, CCL2 and CXCL1) did not differ between lesions with the risk and protective variant (fig. 2, D-F and 3G). Moreover, correlation studies revealed strong positive correlations between NF-κB signaling in astrocytes and expression of chemokines, IL15 and C3, while no correlation was found between NF-κB signaling and GFAP/iNOS expression in astrocytes or $CD68^+$ cell density at the lesion rim (fig. S4).

Since increased astroglial expression of CXCL10, CCL5 and ICAM1 implies enhanced recruitment of lymphocytes, we quantified number of perivascular lymphocytes within MS lesions as well as lesion size in autopsy cases from both groups. We found that both number of infiltrating, perivascular $CD3^+$ T cells (fig. 4A, B) and lesion sizes (fig. 4D) were significantly higher in lesions with the risk variant compared to the protective variant, as was the ratio between perivascular $CD3^+$ T cells and $CD68^+$ microglia at the lesion rim (fig. 4C). We found strong correlations between $CD3^+$ cell infiltration within lesions and astroglial expression of cytosolic p50 ($r = 0.80$) and CXCL10 ($r = 0.67$), and between lesion sizes and astroglial expression of C3d ($r = 0.81$) and

IL15 (r = 0.88) (fig 4E, F; fig S4).

Finally, we examined the effect of the rs7665090 risk variant on white matter lesions in MS patients, as measured by MRI. Since individual lesions can become confluent in advanced MS and are thus difficult to delineate, we quantified overall lesion load per patient rather than individual lesion sizes. We examined a total of 41 and 34 patients homozygous for the risk and protective variant, respectively, from two separate cohorts at the MS Clinics in Yale, USA and Turku, Finland (patient demographics in table S8). Lesion load on fluid-attenuated inversion recovery (FLAIR) images were determined using an automated segmentation algorithm *(22)*, followed by manual correction by three independent raters. We found that the risk variant was associated with a significant increase in lesion load in patients with established disease (fig. 4G-I). Patient age, gender or disease duration did not significantly affect lesion load (table S9).

Discussion. In summary, we demonstrated here in iPSC-derived astrocytes and in astrocytes within MS lesions that the rs7665090 MS risk variant is associated with enhanced NF-κB signaling and upregulation of specific NF-κB targets that drive lymphocyte recruitment and neurotoxicity, implied by increased astroglial expression of C3d *(19)*. Homeostatic and metabolic functions of astrocytes were only moderately affected by the risk variant, but may also contribute to lesion formation by inducing excitotoxicity and metabolic uncoupling from axons/neurons. Consistent with the enhanced chemokine expression by astrocytes, the risk variant was associated with increased lymphocytic infiltration in MS lesions. Moreover, the risk variant was associated with increased lesion sizes in autopsy tissue and increased lesion load on FLAIR images in MS patients.

The substantial impact of the rs7665090 risk variant on astrocytic function, lesion pathology and lesion load is striking, given that this and other susceptibility variants outside of the major histocompatibility complex, confer only minor increases in MS risk *(6)*. The effect seen in MS lesion tissue and on patient MRI might be explained by the combined impact of the risk variant on astrocytes, T cells *(4)* and other immune cells relevant to MS lesion development. Thus, the rs7665090 risk variant may contribute to MS risk through exaggerated astrocytic responses, that

target perturbed peripheral immune processes to the CNS. This can be extended to the general concept that while autoimmunity is the result of risk variant-driven, peripheral immune cell dysfunction, susceptibility to a specific autoimmune disease may be determined by the effect of risk variants on cellular functions in potential target organs.

Our study provides evidence for the first time that genetic variants associated with MS risk directly perturb CNS cell functions. It remains to be shown that risk variants impact on other CNS-constituent cells and possible on non-immune immune pathways, that provide plausible mechanisms for increased MS susceptibility. To this end, a systematic correlation of MS risk variants with detailed chromatin landscapes of CNS cells will provide a platform to delineate the potential relevance of risk variants in different CNS cell types and to identify CNS-intrinsic disease-causing pathways. Therapeutic targeting of variant-dependent, disease causing pathways may be highly effective in MS patients that carry specific variants.

Materials and Methods:

Study Design

The aim of this study was to establish the effect of the rs7665080 risk variant on (i) astrocyte function *in vitro* and *in situ*, (ii) on MS lesion pathology and (iii) on lesion load in MS patients. IPSC-derived astrocytes, autopsied MS cases and MS patients were all homozygous for either the risk or protective variant. We used astrocyte cultures derived from a total of 18 iPSC line obtained from 6 MS patients. For histological lesion analysis, we examined a total of 39 MS lesions from 14 MS patients. All 39 lesions were used to determine lesion sizes; 10 chronic active lesions were selected for their comparable $CD68^{+}$ cell density and used to determine the degree of CD3 infiltration and astrocyte responses. Finally, we identified 93 MS patients homozygous for the risk or protective variant at the MS Clinics in Yale, USA and Turku, Finland, to determine their lesion

load on MRI. We excluded 18 patients from analysis that did not have established disease as defined by either <5 lesions (n=2) and/or <5 years of disease duration or time to treatment with highly effective disease modifying therapies (Tysabri, Rituxan or Lemtrada; n=16), which prevents formation of new lesions. The primary endpoint and exclusion criteria for MS patients were established prospectively. All outlying data were included in the analysis. Primary data of patients' characteristics are provided in tables S5, 7 and 8. Sample sizes were dictated by the availability of MS autopsy cases and of genotyped MS patients. In astrocyte culture, we performed at least three independent experimental replicates. From MS autopsy tissue, we selected lesions with comparable $CD68^+$ densities at the lesion rim and subsequently determined expression levels from at least 20 reactive astrocytes per lesion. Analysis was performed in all experiments in a blinded fashion.

Generation of iPSCs from MS patients and differentiation of iPSCs into astrocytes.

We obtained skin punch biopsies from MS patients at the Yale MS Clinic that were homozygous for the rs7665090 risk variant or protective variant (table S5) and generated explant cultures for derivation of primary human fibroblasts as described *(23)*. Fibroblasts were cultured by Tempo Bioscience, Inc (San Francisco, CA, USA; http://www.tempobioscience.com/), reprogrammed to individual iPSC colonies and expanded, using their proprietary reprogramming protocol. Pluripotency of iPSC lines was confirmed by assessing expression of biomarkers including Oct4, Tra-1-80, Nanog, and SSEA4. IPSC colonies were differentiated into astrocyte progenitors and matured into astrocytes, expressing S100beta and GFAP, using Tempo Bioscience's serum-, feeder-, integration- and genetic elements-free, non-viral technology. For maturation, astrocytes were plated on poly-L-ornithine/laminin and differentiated with DMEM/F12/neurobasal medium (50%/50%) containing 10ng/ml BMP-4 for 2-4 weeks until >90% of the cells were $GFAP^+$ and

GLAST$^+$ as determined by flow cytometry. FACS-sorted GLAST$^+$ astrocytes were used for all experiments.

Chromatin accessibility profiling in iPSC-derived astrocytes.

Human fetal astrocytes (n=2) and iPSC-derived astrocytes (n=4) were profiled for chromatin accessibility using the assay for transposase-accessible chromatin (ATAC-seq) *(15, 24)*. Aliquots of 5,000 cells were incubated with transposase solution containing 1% digitonin *(24)* at 37°C with agitation at 300 rpm for 30 min. After transposition, DNA was purified (MinElute PCR Purification Kit; QIAGEN) and transposed fragments were minimally PCR amplified *(15)* and purified using the Agencourt AMPure XP system (Beckman Coulter). The average fragment size was estimated by Bioanalyzer (Agilent) and libraries were quantitated with the qPCR-based Library Quantification Kit (KAPA Biosystems). Purified libraries were sequenced on the Illumina HiSeq 2000, generating paired-end 100 bp fragments. Fragments were aligned to hg38 with bowtie2 *(25)* and unique, singly mapping reads were retained for further analysis. Visualization tracks were generated by calculating the number of reads aligning at each genomic position and normalizing for library size.

Gene expression profiling in iPSC-derived astrocytes.

Astrocytes were stimulated with 10 ng/ml IL-1β/100 U/ml IFN-γ for 12 hrs and 50 ng/ml TNF-α for an additional 4 hrs before total RNA extraction (RNeasy Micro Plus Kit; Qiagen), reverse transcription (RT^2 First Strand Kit, Qiagen) and gene profiling with a Human NF-κB Signaling Targets RT² Profiler PCR Array (Qiagen), as described before *(9)*.

Flow cytometry, Western Blot and ELISA in iPSC-derived astrocytes.

To assess NF-κB activation with flow cytometry, astrocytes were stimulated with 50ng/ml TNF-α and 10ng/ml IL-1β for 10 min, dissociated with accutase, stained with fluorescent-labeled primary

antibodies (table S6) and analyzed on either a FACSCalibur or a LSRII flow cytometer (BD Biosciences)*(9)*. Protein expression in unstimulated and stimulated (50ng/ml TNF-α/10ng/ml IL-1β, 48 hrs) cultured astrocytes were determined with Western blot as previously described *(9)* with primary antibodies listed in fig. S6. Proteins were visualized with an enhanced chemiluminescence using an ImageQuant LAS 4000 camera (GE Healthcare). Densitometry was performed with ImageJ software and values normalized to loading control (β-actin) were used for analyses. Cytokine release was quantified with sandwich ELISAs (DuoSet ELISA for CXCL10, CCL5, IL-6, R&D Systems; complement C3 ELISA; Abcam). Supernatants from unstimulated and stimulated astrocyte cultures were collected, centrifuged and assayed according to the manufacturer's instructions.

Metabolic assays in iPSC-derived astrocytes.

Glucose uptake was measured in unstimulated and stimulated astrocytes (50ng/ml TNF-α/10 ng/ml IL-1β; 48 hrs) via incorporation of the fluorescent glucose analog 2-NBDG (Thermo Fisher Scientific). 5μM 2-NBDG was added to cells in low glucose medium (1g/L D-Glucose) for 30 min. After washing with HBSS, intracellular fluorescence was determined with an Infinite M1000 fluorescent plate reader (Tecan). Lactate secretion was determined from stimulated and unstimulated cell culture supernatants using a enzymatic assay, which produces a colorimetric (570nm)/fluorometric (λ_{ex}=35nm/λ_{em}=587nm) product proportional to lactate content. (Sigma Aldrich). To quantify glutamate uptake, we incubated astrocyte cultures with HBSS buffer containing 0.5μM L-glutamate and L-[^{3}H]glutamate (1μCi; PerkinElmer) at a 100:1 ratio for 5 min at 37°C. Cells were rapidly moved onto ice, washed twice with ice-cold glutamate-free HBSS buffer and lysed with 0.1N NaOH solution. [^{3}H] radioactivity was measured using a scintillation counter and counts were normalized to total protein levels per sample *(26)*.

Genotyping of formalin-fixed autoptic brain tissue.

Formalin-fixed CNS tissue of 82 MS patients (obtained from the PI's MS tissue bank and the Colorado Brain Bank) was genotyped by isolating DNA using the DNeasy Blood and Tissue Kit and QIAamp DNA FFPE Tissue Kit (both Qiagen). Pre-amplification of DNA and genotyping for rs7665090 was performed with the Taqman PreAmp Master Mix Kit and a Taqman genotyping assay (Applied Biosystems). Genotyping was carried out in duplicates and repeated at least three times in separately obtained DNA samples. We identified 8 cases with the rs7665090-GG and 6 cases with the rs7665090-AA genotype (details in table S7).

Bright-field immunohistochemistry in MS lesions and lesion classification.

For lesion characterization, tissue blocks containing white matter lesions, were sectioned, quenched with 0.03% hydrogen peroxide, incubated with primary antibodies against MBP (myelin), CD68 (myeloid cells) and CD3 (lymphocytes), processed with the appropriate biotinylated secondary antibody and avidin/biotin staining kit with diaminobenzidine as chromogen (Vector ABC Elite Kit, DAB Kit, Vector Laboratories), and counterstained with hematoxylin*(9)*. Controls included isotype antibodies for each primary antibody. White matter lesions were categorized as acute, chronic active and chronic silent. Sizes of all white matter lesion (n=39) were quantified from all 14 cases. In chronic active lesions, we quantified the density of $CD68^+$ cells at the lesion rim and selected 10 chronic active lesions (five cases per group) with comparable CD68 densities (fig. 3A). In these lesions, we counted $CD3^+$ lymphocytes within perivascular infiltrates throughout the lesion area (fig. 4A, B) and examined protein expression in astrocytes (fig. 3C-G).

Immunofluorescence in MS lesions.

To visualize protein expression in reactive astrocytes within lesions, sections were incubated with primary antibodies, listed in table S6, overnight at 4°C, processed with HRP-conjugated secondary antibodies for 2hrs at RT and reacted with Alexa Fluor tyramide (Life Technologies) for 10 min. Subsequently, sections were dyed with 0.7% Sudan Black and $CuSO_4$ to quench auto-fluorescence and counterstained with DAPI. Sections were examined and images acquired on an UltraVIEW VoX (Perkin Elmer) spinning disc confocal Nikon Ti-E Eclipse microscope using the Volocity 6.3 software (Improvision). Images were processed with the ImageJ software *(27)*. Cytosolic and nuclear expression of NF-κB p50 and p65 and chemokine expression levels of CCL2, CCL5, CXCL1, CXCL10, as well as ICAM1, IL-15, complement factor C3, iNOS and GFAP were quantified by densitometric analysis of fluorescent immunoreactivity of GFAP-positive hypertrophic astrocytes at the lesion rim. Acquisition and analysis were performed in a blinded manner.

MRI acquisition and T2 FLAIR lesion segmentation

MRI scans were acquired on a 3T Siemens Skyra scanner (Yale) and 3T Philipps Ingenuity TF PET/MR scanner or a Philips Gyroscan Intera 1.5 T Nova Dual scanner (Turku). Automated lesion detection was performed on T2 weighted fluid attenuated inversion recovery (FLAIR) sequences with the LPA algorithm available as part of the lesion segmentation toolbox (LST) (http://www.applied-statistics.de/lst.htm) *(21)*, followed by manual correction using itk-SNAP software version 3.x by three reviewers blinded to the patients' genotype.

Statistical analysis.

Data represent means ± standard deviation from three independent experiments. Group comparisons of two samples were carried out by *unpaired student's t-tests*. Comparisons of up to four groups were analyzed by *one-way ANOVA* followed by the Tukey-Kramer multiple

comparison *test.* For correlation analysis Pearson correlation coefficients were computed. All values passed the D'Agostino-Pearson omnibus normality test for Gaussian distribution. * $p<0.05$, ** $p<0.01$, *** $p<0.001$ and **** $p<0.0001$. The effect of the risk variant on total lesion load was assessed by applying a logarithmic transformation in order to better approximate a normal distribution of lesion load values *(28)*. To account for confounding factors, we fitted a multivariate linear regression model log (lesion load) that included age, gender, disease duration, and genetic variant. The effects of each factor were assessed by F test (ANOVA) (table S9).

References and Notes:

1. A. Nylander, D. A. Hafler, Multiple sclerosis, *J. Clin. Invest.* **122**, 1180–1188 (2012).

2. The International Multiple Sclerosis Genetics Consortium (IMSGC), The Multiple Sclerosis Genomic Map: Role of peripheral immune cells and resident microglia in susceptibility. *https://www.biorxiv.org/content/early/2017/07/13/143933*.

3. K. K.-H. Farh, A. Marson, J. Zhu, M. Kleinewietfeld, W. J. Housley, S. Beik, N. Shoresh, H. Whitton, R. J. H. Ryan, A. A. Shishkin, M. Hatan, M. J. Carrasco-Alfonso, D. Mayer, C. J. Luckey, N. A. Patsopoulos, P. L. De Jager, V. K. Kuchroo, C. B. Epstein, M. J. Daly, D. A. Hafler, B. E. Bernstein, Genetic and epigenetic fine mapping of causal autoimmune disease variants, *Nature Publishing Group* **518**, 337–343 (2015).

4. W. J. Housley, S. D. Fernandez, K. Vera, S. R. Murikinati, J. Grutzendler, N. Cuerdon, L. Glick, P. L. De Jager, M. Mitrovic, C. Cotsapas, D. A. Hafler, Genetic variants associated with autoimmunity drive NFκB signaling and responses to inflammatory stimuli, *Sci Transl Med* **7**, 291ra93–291ra93 (2015).

5. M. S. Hayden, S. Ghosh, NF-κB, the first quarter-century: remarkable progress and outstanding questions, *Genes & Development* **26**, 203–234 (2012).

6. I. M. S. G. C. IMSGC, Analysis of immune-related loci identifies 48 new susceptibility variants for multiple sclerosis, *Nat Genet* **45**, 1353–1360 (2013).

7. E. H. Wilson, W. Weninger, C. A. Hunter, Trafficking of immune cells in the central nervous system, *J. Clin. Invest.* **120**, 1368–1379 (2010).

8. M. V. Sofroniew, Astrocyte barriers to neurotoxic inflammation, **16**, 249–263 (2015).

9. G. Ponath, S. Ramanan, M. Mubarak, W. Housley, S. Lee, F. R. Sahinkaya, A. Vortmeyer, C. S. Raine, D. Pitt, Myelin phagocytosis by astrocytes after myelin damage promotes lesion pathology, **140**, 399–413 (2017).

10. C. F. Brosnan, C. S. Raine, The astrocyte in multiple sclerosis revisited, *Glia* **61**, 453–465 (2013).

11. R. Brambilla, T. Persaud, X. Hu, S. Karmally, V. I. Shestopalov, G. Dvoriantchikova, D. Ivanov, L. Nathanson, S. R. Barnum, J. R. Bethea, Transgenic Inhibition of Astroglial NF-κB Improves Functional Outcome in Experimental Autoimmune Encephalomyelitis by Suppressing Chronic Central Nervous System Inflammation, *The Journal of Immunology* **182**, 2628–2640 (2009).

12. R. Brambilla, P. D. Morton, J. J. Ashbaugh, S. Karmally, K. L. Lambertsen, J. R. Bethea, Astrocytes play a key role in EAE pathophysiology by orchestrating in the CNS the inflammatory response of resident and peripheral immune cells and by suppressing remyelination, *Glia* **62**, 452–467 (2014).

13. I. Dunham, A. Kundaje, S. F. Aldred, P. J. Collins, C. A. Davis, F. Doyle, C. B. Epstein, S. Frietze, J. Harrow, R. Kaul, J. Khatun, B. R. Lajoie, S. G. Landt, B. K. Lee, F. Pauli, K. R. Rosenbloom, P. Sabo, A. Safi, A. Sanyal, N. Shoresh, J. M. Simon, L. Song, N. D. Trinklein, R. C. Altshuler, E. Birney, J. B. Brown, C. Cheng, S. Djebali, X. Dong, J. Ernst, T. S. Furey, M. Gerstein, B. Giardine, M. Greven, R. C. Hardison, R. S. Harris, J. Herrero, M. M. Hoffman, S. Iyer, M. Kellis, P. Kheradpour, T. Lassmann, Q. Li, X. Lin, G. K. Marinov, A. Merkel, A. Mortazavi, S. C. J. Parker, T. E. Reddy, J. Rozowsky, F. Schlesinger, R. E. Thurman, J. Wang, L. D. Ward, T. W. Whitfield, S. P. Wilder, W. Wu, H. S. Xi, K. Y. Yip, J. Zhuang, B. E. Bernstein, E. D. Green, C. Gunter, M. Snyder, M. J. Pazin, R. F. Lowdon, L. A. L. Dillon, L. B. Adams, C. J. Kelly, J. Zhang, J. R. Wexler, P. J. Good, E. A. Feingold, G. E. Crawford, J. Dekker, L. Elnitski, P. J. Farnham, M. C. Giddings, T. R. Gingeras, R. Guigó, T. J. Hubbard, W. J. Kent, J. D. Lieb, E. H. Margulies, R. M. Myers, An integrated encyclopedia of DNA elements in the human genome, *Nature* **489**, 57–74 (2012).

14. 1000 Genomes Project Consortium, G. R. Abecasis, A. Auton, L. D. Brooks, M. A. DePristo, R. M. Durbin, R. E. Handsaker, H. M. Kang, G. T. Marth, G. A. McVean, An integrated map of genetic variation from 1,092 human genomes, *Nature Publishing Group* **491**, 56–65 (2012).

15. J. D. Buenrostro, P. G. Giresi, L. C. Zaba, H. Y. Chang, W. J. Greenleaf, Transposition of native chromatin for fast and sensitive epigenomic profiling of open chromatin, DNA-binding proteins and nucleosome position, *Nat Meth* **10**, 1213–1218 (2013).

16. K. Selmaj, C. S. Raine, B. Cannella, C. F. Brosnan, Identification of lymphotoxin and tumor necrosis factor in multiple sclerosis lesions, *J. Clin. Invest.* **87**, 949–954 (1991).

17. S. M. Burm, L. A. N. Peferoen, E. A. Zuiderwijk-Sick, K. G. Haanstra, B. A. t Hart, P. Van Der Valk, S. Amor, J. Bauer, J. J. Bajramovic, Expression of IL-1β in rhesus EAE and MS lesions is mainly induced in the CNS itself, *J Neuroinflammation* **13**, 519 (2016).

18. U. Traugott, P. Lebon, Multiple sclerosis: Involvement of interferons in lesion pathogenesis, *Ann Neurol.* **24**, 243–251 (1988).

19. S. A. Liddelow, K. A. Guttenplan, L. E. Clarke, F. C. Bennett, C. J. Bohlen, L. Schirmer, M. L. Bennett, A. E. Münch, W.-S. Chung, T. C. Peterson, D. K. Wilton, A. Frouin, B. A. Napier, N. Panicker, M. Kumar, M. S. Buckwalter, D. H. Rowitch, V. L. Dawson, T. M. Dawson, B. Stevens, Ben A Barres, Neurotoxic reactive astrocytes are induced by activated microglia, *Nature Publishing Group*, 1–25 (2017).

20. J. Fang, D. Han, J. Hong, Q. Tan, Y. Tian, The chemokine, macrophage inflammatory protein-2γ, reduces the expression of glutamate transporter-1 on astrocytes and increases neuronal sensitivity to glutamate excitotoxicity, *J Neuroinflammation* **9**, 5–1 (2012).

21. J. Li, T. D. Gould, P. Yuan, H. K. Manji, G. Chen, Post-mortem Interval Effects on the Phosphorylation of Signaling Proteins, *Neuropsychopharmacology*, 1–9 (2002).

22. P. Schmidt, C. Gaser, M. Arsic, D. Buck, A. Förschler, A. Berthele, M. Hoshi, R. Ilg, V. J. Schmid, C. Zimmer, B. Hemmer, M. Mühlau, An automated tool for detection of FLAIR-hyperintense white-matter lesions in Multiple Sclerosis, *NeuroImage* **59**, 3774–3783 (2012).

23. M. Vangipuram, D. Ting, S. Kim, R. Diaz, B. Schüle, Skin punch biopsy explant culture for derivation of primary human fibroblasts, *J Vis Exp*, e3779–e3779 (2013).

24. M. R. Corces, J. D. Buenrostro, B. Wu, P. G. Greenside, S. M. Chan, J. L. Koenig, M. P. Snyder, J. K. Pritchard, A. Kundaje, W. J. Greenleaf, R. Majeti, H. Y. Chang, Lineage-specific and single-cell chromatin accessibility charts human hematopoiesis and leukemia evolution, *Nat Genet* **48**, 1193–1203 (2016).

25. B. Langmead, S. L. Salzberg, Fast gapped-read alignment with Bowtie 2, *Nat Meth* **9**, 357–359 (2012).

26. D. Pitt, I. E. Nagelmeier, H. C. Wilson, C. S. Raine, Glutamate uptake by oligodendrocytes: Implications for excitotoxicity in multiple sclerosis, *Neurology* **61**, 1113–1120 (2003).

27. C. A. Schneider, W. S. Rasband, K. W. Eliceiri, NIH Image to ImageJ: 25 years of image analysis, *Nat Meth* **9**, 671–675 (2012).

28. R. Ghassemi, S. Narayanan, B. Banwell, J. G. Sled, M. Shroff, D. L. Arnold, Canadian Pediatric Demyelinating Disease Network, C. Lenglet, Ed. Quantitative determination of regional lesion volume and distribution in children and adults with relapsing-remitting multiple sclerosis, *PLoS ONE* **9**, e85741 (2014).

Acknowledgments: D.P. is supported by the National Multiple Sclerosis Society (RG-1610-26049), by the National Institutes of Health Grant R01 NS102267 and by a generous gift from Stanley Trottman. D.A.H. is supported by National Institutes of Health Grants P01 AI045757, U19 AI046130, U19 AI070352, and P01 AI039671, and the Nancy Taylor Foundation for Chronic Diseases. M.L. is supported by an endMS Postdoctoral Fellowship Award from the Multiple Sclerosis Society of Canada. T.S. is supported by the Banyu Fellowship Program and Uehara Research Fellowship Program. L.A. is supported by the Finnish Academy, the Sigrid Juselius Foundation and a Grant for Multiple Sclerosis Innovation by MerckSerono. T.D.N is supported by the National Multiple Sclerosis Society grant RG-1602-07671 and the National Institutes of Health grant R01 NS090464.

Sequencing service was conducted at Yale Stem Cell Center Genomics Core facility which was supported by the Connecticut Regenerative Medicine Research Fund and the Li Ka Shing Foundation. We would like to acknowledge the Rocky Mountain Multiple Sclerosis Center Tissue Bank for contributing *post mortem* MS brain tissue for this study.

Figures

Figure 1 Chromatin accessibility in the *NFKB1/MANBA* risk haplotype block in astrocytes and T cells

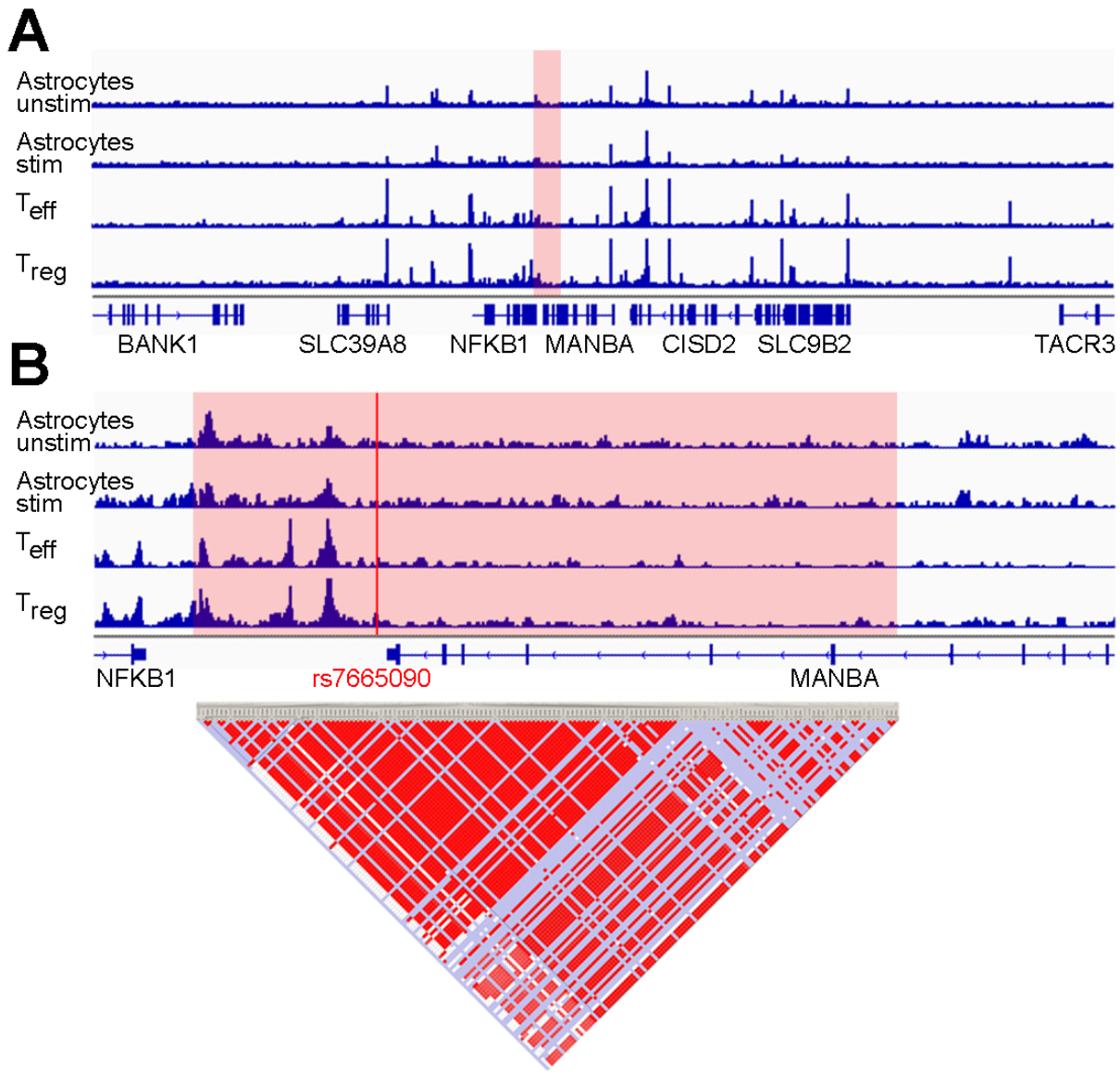

Figure 1. Chromatin accessibility in the *NFKB1/MANBA* risk haplotype block in astrocytes and T cells. (**A**) Normalized ATAC-seq profiles in the *NFKB1/MANBA* risk locus are similar in unstimulated and stimulated human fetal astrocytes (AC_{unstim} and AC_{stim}; first two tracks) and in *ex vivo* unstimulated effector and regulatory T cells (T_{eff} and T_{reg}; third and fourth track). The height of the bar graph at each point represents the number of unique, singly-mapping reads at each genomic position; each track is normalized for library size. The *NFKB1/MANBA* haploblock is shaded in red. The genomic coordinates are chr4:101,796383-103694,281. (**B**) Higher magnification (chr4:102,614,123-102,674,492) of the risk haploblock, shaded in red, shows accessible chromatin mostly in the intergenic region between *NFKB1* and *MANBA* with comparable ATAC-seq profiles in astrocytes and T cells. The location of the tagging SNP rs7665090 is indicated by the red line. Pairwise linkage disequilibrium (D') values between SNPs in the CEU population of the 1000 Genomes Project are indicated below (red indicates D'>0.95).

Figure 2 Effect of the rs7665080-G risk variant on activated human iPSC-derived astrocytes

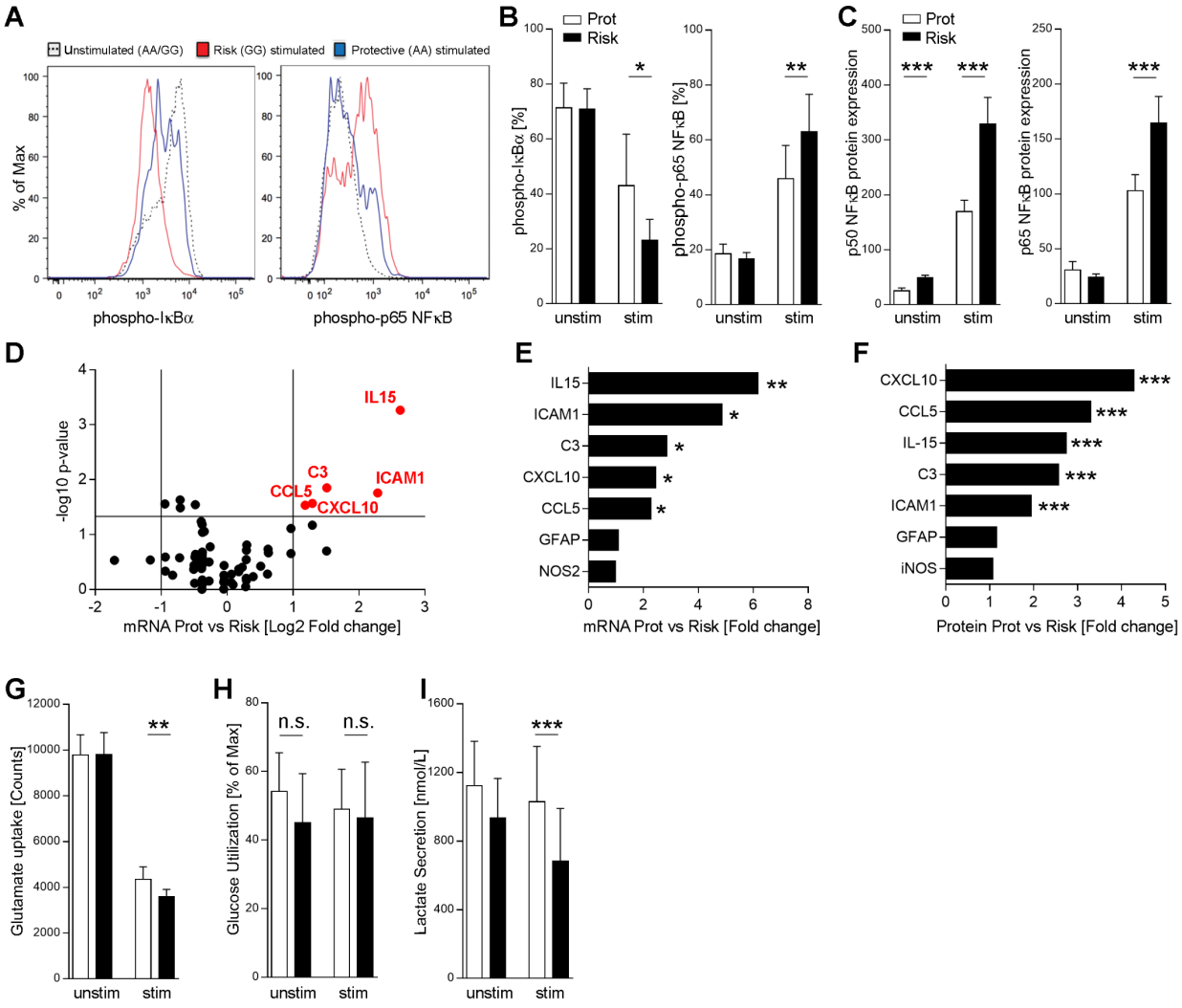

Figure 2. Effect of the rs7665080-G risk variant on activated human iPSC-derived astrocytes. (**A**, **B**) Degradation of IκBα and phosphorylation of p65 in iPSC-derived astrocytes with risk and protective variant at a resting state and after 10 min of stimulation with TNFα (50 ng/ml) and IL-1β (10 ng/ml) by flow cytometry. (**C**) Expression of p50 and p65 in unstimulated and stimulated (10 ng/ml IL-1β; 100 U/ml IFNγ for 12 hrs, followed by 50 ng/ml TNFα for 4 hrs) iPSC-derived astrocytes from both groups by Western blot. (**D**-**E**) Volcano plot profiling astroglial expression of 84 *NFKB* target genes after stimulation with IL-1β, IFNγ and TNFα. Red dots indicate genes with ≥2-fold expression and *p*-values ≤0.05. Genes with significantly increased expression are listed in (**E**) and corresponding protein expression in (**F**). (**G**) Uptake of L-[3,4-^{3}H] glutamic acid by iPSC-derived unstimulated and stimulated (with IL-1β, IFNγ and TNFα) astrocytes with risk and protective variant. (**H**, **I**) Glucose uptake and lactate secretion by astrocytes with the risk and protective variant. Data represent means ± s.d. from three independent experiments. P values shown for one-way ANOVA, and *post hoc* Tukey–Kramer test. * $p<0.05$, ** $p<0.01$ and *** $p<0.001$.

Figure 3 Effect of the rs7665080-G risk variant on hypertrophic astrocytes in white matter MS lesions

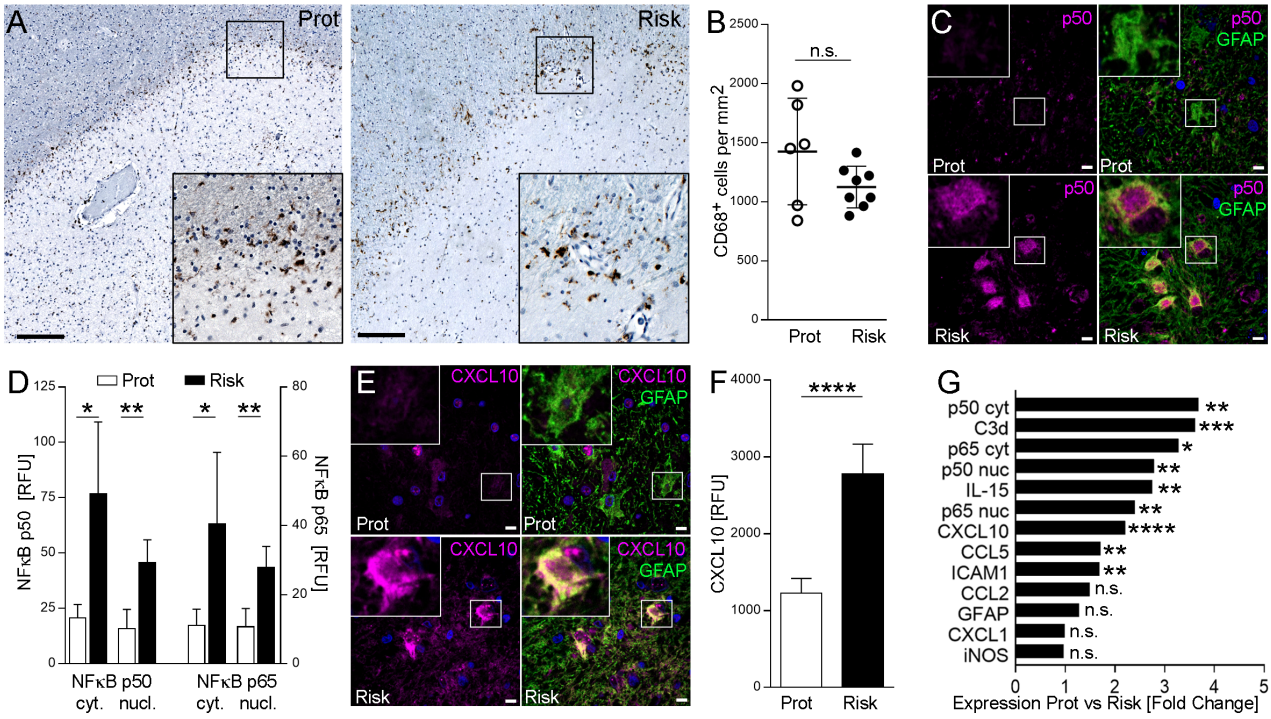

Figure 3. Effect of the rs7665080-G risk variant on hypertrophic astrocytes in white matter MS lesions. (**A**) Chronic active MS lesions from autopsy cases with the rs7665080 risk and protective variant. Staining for CD68 (brown) shows activated microglia at the lesion rim. Counterstain with hematoxylin (blue). Magnifications in inset. (**B**) Quantification of $CD68^+$ cell densities in14 lesions from 10 MS cases (five per group). Dots represent average cell densities per lesion counted per group. (**C**) Confocal microscopy images of hypertrophic astrocytes at the lesion edge labeled with fluorescent antibodies against p50 (magenta) and GFAP (green); counterstained with Hoechst 33342. (**D**) Densitometric quantification of NF-κB p50 and p65 in the cytosol/nucleus of hypertrophic lesional astrocytes (5 cases per group). (**E**) Hypertrophic astrocytes stained with fluorescent antibodies against CXCL10 (magenta) and GFAP (green); counterstained with Hoechst 33342. (**F**) Quantification of CXCL10 in hypertrophic $GFAP^+$ astrocytes (5 cases per group). (**G**) Differential expression of immune mediators and activation markers in astrocytes from both groups. Data represent means ± s.d. P values shown for one-way ANOVA, and *post hoc* Tukey–Kramer test. * $p<0.05$, ** $p<0.01$ and *** $p<0.001$. Scale bar = 100 μm in A, 15 μm in C, E.

Figure 4 Effect of the rs7665080-G risk variant on lesion pathology and lesion load in MS patients

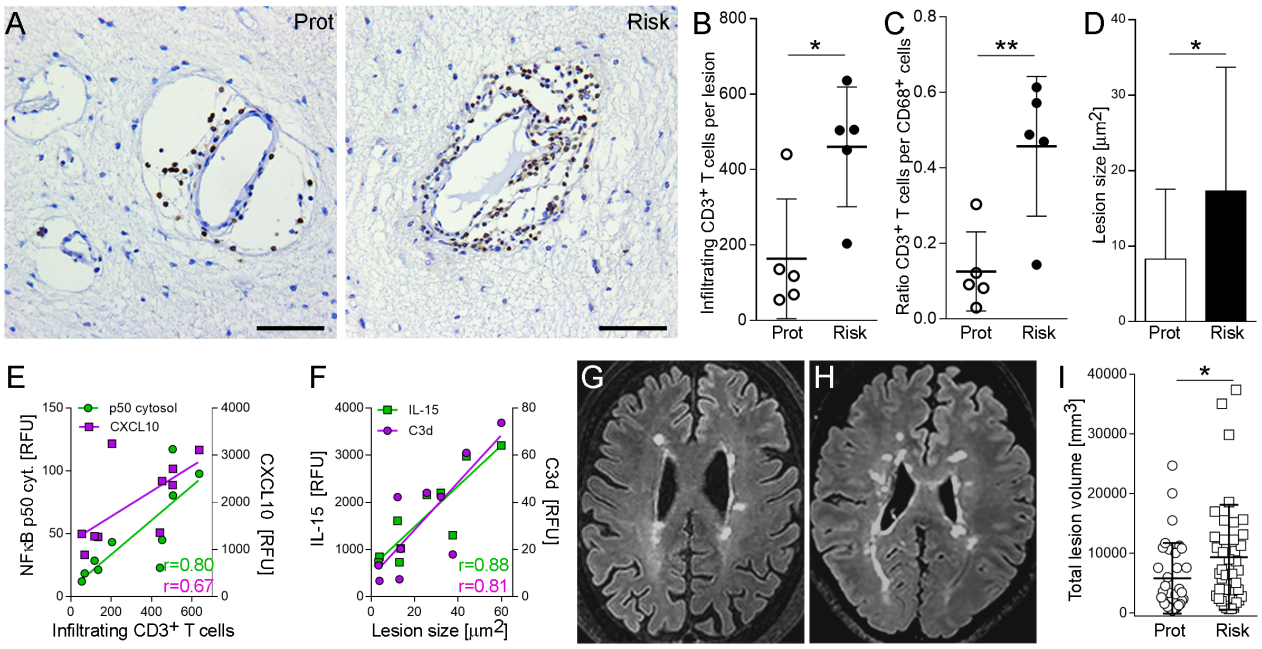

Figure 4. Effect of the rs7665080-G risk variant on lesion pathology and lesion load in MS patients. (**A**) Bright-field images of perivascular infiltrates within chronic active MS lesions labeled with anti-CD3 antibody. (**B**) Quantification of infiltrating, perivascular $CD3^+$ T cells in 10 lesions from five MS cases per group. Dots represent average $CD3^+$ cells. (**C**) Ratio of $CD3^+$ cells per $CD68^+$ cells in lesions from both groups. (**D**) Quantification of lesion sizes determined as areas of demyelination in MBP-stained sections (18 lesions from 6 cases (protective) and 21 lesions from 8 cases (risk)). (**E**) Correlation of infiltrating $CD3^+$ cells with cytosolic NF-κB p50 (r=0.80, p=0.005) and CXCL10 (r=0.67, p=0.036) expression. (**F**) Correlation of lesion size with IL-15 (r=0.88, p=0.001) and C3d (r=0.81, p= 0.005). **(G, H)** Examples of white matter lesions on FLAIR images from MS patients homozygous for the protective (G) and risk variant (H). **(I)** Total lesion volumes of 35 MS patients (rs7665080-GG) and 40 patients (rs7665080-AA) with established disease (≥5 years disease duration). Data represent means ± s.d. p values shown for one-way ANOVA and *post hoc* Tukey–Kramer test (B, C, D) or F-Test (I). * $p<0.05$ and ** $p<0.01$. Scale bar=50µm.